

CEBAF



0205 9100 017 096 9

**CEBAF**

The Continuous Electron Beam Accelerator Facility

Theory Group Preprint Series

CEBAF-TH-94-16

Additional copies are available from the authors.

MONTE CARLO APPROACHES TO THE FEW-NUCLEON  
CONTINUUM

R. Schiavilla

*Department of Physics, Old Dominion University, Norfolk, VA 23529  
and  
CEBAF Theory Group, Newport News, VA 23606*

J. Carlson

*Theory Division, Los Alamos National Laboratory, Los Alamos, NM 87545*

R. B. Wiringa

*Physics Division, Argonne National Laboratory, Argonne, IL 60439*

DISCLAIMER

This report was prepared as an account of work sponsored by the United States government. Neither the United States nor the United States Department of Energy, nor any of their employees, makes any warranty, express or implied, or assumes any legal liability or responsibility for the accuracy, completeness, or usefulness of any information, apparatus, product, or process disclosed, or represents that its use would not infringe privately owned rights. Reference herein to any specific commercial product, process, or service by trade name, mark, manufacturer, or otherwise, does not necessarily constitute or imply its endorsement, recommendation, or favoring by the United States government or any agency thereof. The views and opinions of authors expressed herein do not necessarily state or reflect those of the United States government or any agency thereof.

# MONTE CARLO APPROACHES TO THE FEW-NUCLEON CONTINUUM

R. Schiavilla

*Physics Department, Old Dominion University, Norfolk, VA 23529*

and

*CEBAF Theory Group, Newport News, VA 23606*

J. Carlson

*Theory Division, Los Alamos National Laboratory, Los Alamos, NM 87545*

R.B. Wiringa

*Physics Division, Argonne National Laboratory, Argonne, IL 60439*

## ABSTRACT

Variational and Green's Function Monte Carlo methods are reviewed as applied to the study of the few-nucleon continuum at low- and intermediate-energies. Results recently obtained for the radiative and weak capture reactions  $n + {}^3\text{He} \rightarrow {}^4\text{He} + \gamma$  and  $p + {}^3\text{He} \rightarrow {}^4\text{He} + e^+ + \nu_e$ , the  ${}^5\text{He}$  P-wave resonances, and the inclusive and exclusive electron scattering reactions on  ${}^3\text{H}$  and the helium isotopes are summarized.

## INTRODUCTION

In recent years great progress has been made in the description of few-nucleon systems with a variety of different techniques. Accurate ground state wave functions for the  $A=3$  and 4 nuclei have been obtained from realistic Hamiltonians with Faddeev [1-3], Yakubovsky [2], and Correlated Hyperspherical Harmonics [4,5] methods. These techniques have also been generalized to successfully describe the three- and four-nucleon continuum at very low energies [6,7]. However, at moderately high excitation energies the number of channels to be included for converged solutions is very large. Indeed, reliable solutions of the Faddeev equations up to 100 MeV energies have only very recently become available [8].

Monte Carlo methods have been applied to a variety of strongly interacting many-body systems in condensed matter [9] and nuclear [10] physics, and lattice quantum chromodynamics [11]. The present contribution is an overview of how Variational and Green's Function Monte Carlo techniques, in particular, are used to describe bound and continuum spectra of few-nucleon systems. The theoretical

framework, the methods involved in the treatment of the continuum (our focus here), and the results obtained to date for both low- and high-energy continuum properties are reviewed.

## HAMILTONIAN AND CURRENTS

In the non-relativistic many-body theory of nuclei, the Hamiltonian governing the nucleons' dynamics is taken as the sum of a kinetic energy, two- and three-nucleon interaction terms:

$$H = \sum_i t_i + \sum_{i<j} v_{ij} + \sum_{i<j<k} V_{ijk} . \quad (1)$$

The two-nucleon interaction is written as

$$v_{ij} = v_{ij}^R + v_{ij}^\pi , \quad (2)$$

where  $v_{ij}^\pi$  is the long-range one-pion-exchange potential (OPEP)

$$v_{ij}^\pi = [v^{\sigma\tau}(r_{ij})\sigma_i \cdot \sigma_j + v^{t\tau}(r_{ij})S_{ij}]\tau_i \cdot \tau_j , \quad (3)$$

$\sigma$  ( $\tau$ ) being the standard Pauli spin (isospin) matrices and  $S_{ij}$  the tensor operator. The radial functions  $v^{\sigma\tau}(r)$  and  $v^{t\tau}(r)$  reduce to  $\exp(-\mu r)/(\mu r)$  and  $[1+3/(\mu r) + 3/(\mu r)^2]\exp(-\mu r)/(\mu r)$ , respectively, when the interparticle distance  $r \gtrsim \mu^{-1}$  ( $\approx 1.4$ ) fm. The effects due to all other subnucleonic degrees of freedom, such as those associated with heavy mesons and nucleonic resonances or quarks and gluons, are

absorbed into  $v_{ij}^R$ . This part of the interaction has a short range  $r \lesssim \mu^{-1}$ , and is characterized by a complicated spin-isospin structure

$$v_{ij}^R = \sum_p v^{(p)}(r_{ij}) O_{ij}^p, \quad (4)$$

$$O_{ij}^p = [1, \sigma_i \cdot \sigma_j, S_{ij}, (\mathbf{L} \cdot \mathbf{S})_{ij}, \dots] \otimes [1, \tau_i \cdot \tau_j], \quad (5)$$

$\mathbf{L}$  and  $\mathbf{S}$  being the relative orbital angular momentum and the total spin of the pair, respectively. It is constrained by fitting nucleon-nucleon elastic scattering data in the laboratory energy range 0–350 MeV and deuteron properties. The first eight operators listed above are common to all current, realistic models of  $v_{ij}$ . The additional operators not shown above include terms quadratic in the relative momentum  $\mathbf{p}$ , such as in the Paris [12] and Bonn [13] interactions, or quadratic in  $\mathbf{L}$ , such as in the Urbana [14] and Argonne [15] interactions.

The two outstanding features of the  $v_{ij}$  are its short-range repulsion and long-range tensor character. These components induce important short-range and tensor correlations among the nucleons in nuclei. Indeed, one primary motivation of few-body nuclear physics is the theoretical and experimental investigation of these correlations. All the calculations reported in the present contribution have been carried out with the Argonne  $v_{14}$  interaction [15] and a simplified version of it denoted as Argonne  $v_8$  [16]. This latter interaction does not contain terms quadratic in  $\mathbf{L}$ , and is designed to exactly reproduce the deuteron properties and S- and P-wave phase shifts, as calculated with the full Argonne  $v_{14}$ . The reason for using the  $v_8$  model rather than the more complete  $v_{14}$  is that terms quadratic in  $\mathbf{L}$  (or  $\mathbf{p}$ ) are difficult to handle in simple Green's Function Monte Carlo (GFMC) schemes, as they essentially correspond to different effective masses in each two-body channel. However, these terms are small in the  $v_{14}$  model. In perturbation theory they are found to provide 0.15 MeV and 0.9 MeV extra binding energy in the A=3 and 4 systems, respectively.

The three-nucleon interaction (TNI)  $V_{ijk}$  consists of an attractive term due to two-pion exchange with excitation of an intermediate  $\Delta$ -resonance, and a repulsive phenomenological central term containing no spin-isospin structure. The strengths of these two terms are determined by fitting the binding energies of  $^3\text{H}$  and  $^4\text{He}$  in (essentially) exact Faddeev [1] and GFMC [17] calculations, and the saturation properties of nuclear matter in variational calculations based on chain summation techniques [18]. The Urbana model-VIII is used in most of the results discussed in the present work. Together with the Argonne  $v_{14}$  it reproduces the empirical binding energies of  $^3\text{H}$  and  $^4\text{He}$  and the equilibrium density of nuclear

matter [19]. However, the binding energy per nucleon in nuclear matter is underpredicted by roughly 15%. It should be emphasized that the TNI, while it provides a significant fraction of the nuclear binding, has an expectation value which is only a few percent of the two-nucleon interaction.

One motivation for introducing the TNI in the nuclear Hamiltonian is that all presently available realistic two-nucleon interactions, with the exception of one of the Bonn interactions [13], underpredict the empirical binding energies of light nuclei. Obviously, this does not imply that the TNI alone is responsible for the binding energy defect in nuclei. Other effects, including the non-localities associated with the extended (non point-like) nature of the nucleons and relativistic corrections, need to be investigated. Many of these effects are related, and studies of their importance are still in their infancy.

In order to study the response of nuclei to an electromagnetic probe within the present approach, the nuclear charge and current densities are represented by effective operators that operate on the nucleon degrees of freedom. These operators are expanded into sums of one-, two- and many-body terms:

$$\rho(\mathbf{q}) = \sum_i \rho_i^{(1)} + \sum_{i<j} \rho_{ij}^{(2)} + \dots, \quad (6)$$

$$\mathbf{j}(\mathbf{q}) = \sum_i \mathbf{j}_i^{(1)} + \sum_{i<j} \mathbf{j}_{ij}^{(2)} + \dots. \quad (7)$$

The one-body terms  $\rho^{(1)}$  and  $\mathbf{j}^{(1)}$  have the standard impulse approximation form, while the two-body terms  $\rho^{(2)}$  and  $\mathbf{j}^{(2)}$  consist of “model-independent” and “model-dependent” parts [20–22] (the expansions of the couplings above are truncated at the two-body level in the results discussed here). The “model-independent”  $\mathbf{j}^{(2)}$  terms do not have any free parameters, are determined by the interaction  $v_{ij}$ , and are necessary to satisfy the continuity equation. The “model-dependent”  $\mathbf{j}^{(2)}$  terms, such as those associated with the  $\Delta$ -excitation,  $\rho\pi\gamma$  and  $\omega\pi\gamma$  mechanisms, are purely transverse and therefore unconstrained by the  $v_{ij}$ . Furthermore, they depend on a set of only approximately known cutoff parameters and coupling constants. Their contribution for momentum transfers  $\lesssim 1$  GeV/c is small when compared to that of the leading “model-independent” two-body currents, and will not be discussed further here [20,19].

The most important of the “model-independent” two-body currents is that associated with the  $v^{i\tau}(r_{ij})S_{ij}\tau_i \cdot \tau_j$  and  $v^{\sigma\tau}(r_{ij})\sigma_i \cdot \sigma_j \tau_i \cdot \tau_j$  interactions in  $v_{ij}$ . The corresponding current operator is given by:

$$\mathbf{j}_{PS}^{(2)}(\mathbf{q}) = G_E^V(q_\mu^2) \sum_{i<j} -i(\tau_i \times \tau_j)_z \left\{ v_{PS}(k_j) \sigma_i (\sigma_j \cdot \mathbf{k}_j) - v_{PS}(k_i) \sigma_j (\sigma_i \cdot \mathbf{k}_i) \right\}$$

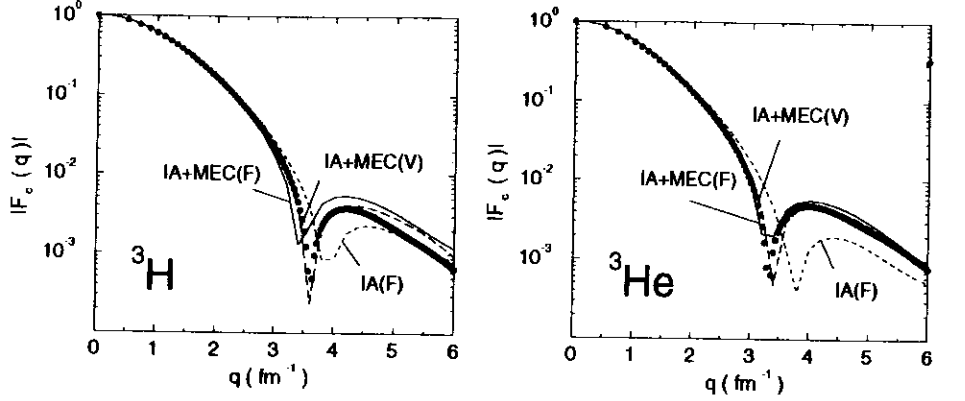
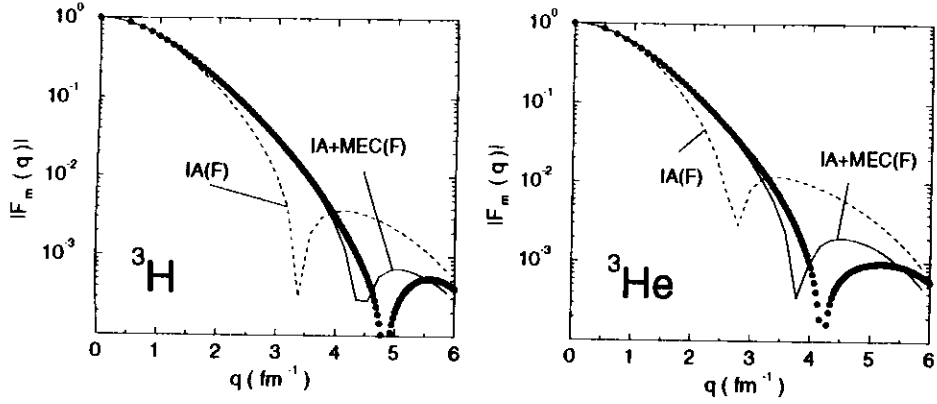


FIG. 1. The  ${}^3\text{H}$  and  ${}^3\text{He}$  magnetic (top panels) and charge (bottom panels) form factors.

$$-\frac{\mathbf{k}_i - \mathbf{k}_j}{k_i^2 - k_j^2} \{ v_{PS}(k_j) - v_{PS}(k_i) \} (\boldsymbol{\sigma}_i \cdot \mathbf{k}_i) (\boldsymbol{\sigma}_j \cdot \mathbf{k}_j) \} , \quad (8)$$

where  $\mathbf{q} = \mathbf{k}_i + \mathbf{k}_j$ ,  $G_E^V$  is the isovector combination of the nucleon electric form factors (evaluated at the four momentum transfer  $q_\mu^2 = q^2 - \omega^2$ ,  $\omega$  being the energy transfer), and  $v_{PS}$  is projected out from the radial parts of the  $v^{\sigma\tau}$  and  $v^{t\tau}$  components

$$v_{PS}(k) = 2v^{t\tau}(k) - v^{\sigma\tau}(k) . \quad (9)$$

A detailed discussion of these currents, along with their explicit expressions, can be found in refs. [20,21]. Here we only note that the  $\mathbf{j}_{PS}^{(2)}$  gives by far the largest contribution to isovector observables in the two- and three-body systems, such as the electrodisintegration at threshold of the deuteron [23] and the magnetic form factors of the trinucleons [19]. The currents due to the explicit momentum dependence of the  $v_{ij}$  are predominantly isoscalar in character, and give significant contribution to the  $B$  structure function of the deuteron [23], and isoscalar combination of the magnetic form factors of the trinucleons [19].

The most important two-body charge operator can be derived by considering the non-relativistic reduction of the virtual pion photoproduction amplitude [22]. We obtain:

$$\rho_{PS}^{(2)}(\mathbf{q}) = \sum_{i < j} \frac{3}{2m} [F_1^S(q_\mu^2) \boldsymbol{\tau}_i \cdot \boldsymbol{\tau}_j + F_1^V(q_\mu^2) \tau_{j,z}] v_{PS}(k_j) (\boldsymbol{\sigma}_i \cdot \mathbf{q}) (\boldsymbol{\sigma}_j \cdot \mathbf{k}_j) + i \rightleftharpoons j, \quad (10)$$

where  $F_1^{S,V}$  are the isoscalar and isovector combinations of the Dirac nucleon form factors (normalized as  $F_1^S(0) = F_1^V(0) = 1$ ). It is determined by the  $v_{ij}$ , and

hence is to be considered “model-independent”. The two-body charge operators are to be viewed as relativistic corrections proportional to  $1/m^2$ , where  $m$  is the nucleon mass. For consistency, we also include the Darwin-Foldy and spin-orbit relativistic corrections to the single-nucleon charge operator.

The results obtained within the present theoretical framework (Argonne  $v_{14}$  and Urbana model-VIII) for the charge and magnetic form factors of  ${}^3\text{H}$  and  ${}^3\text{He}$  [19], the charge form factor [19] and longitudinal-longitudinal distribution function (LLDF) of  ${}^4\text{He}$  [24] are displayed in Figs. 1-2. The LLDF is defined as

$$\rho_{LL}(q) = \frac{1}{Z} \langle 0 | \rho^1(\mathbf{q}) \rho(\mathbf{q}) | 0 \rangle - 1 , \quad (11)$$

where  $|0\rangle$  is the ground state of the nucleus. Inclusive ( $e,e'$ ) data on the longitudinal response function and the measured charge form factor provide information on the empirical LLDF. The unmeasured strength in the tail of the response limits the accuracy of the analysis, though, as reflected by the large errors in Fig. 2.

The agreement between theory and experiment is satisfactory at low and moderate values of momentum transfers ( $q \lesssim 600$  MeV/c). However, the calculated zeros of the trinucleon magnetic form factors are shifted to lower  $q$  than the data indicate. It will be interesting to calculate these observables with the more recent Argonne  $v_{18}$  interaction model [25], which incorporates charge-independence-breaking components and a significantly weaker tensor force than the older Argonne  $v_{14}$ . It will also be interesting to explore the effects due to

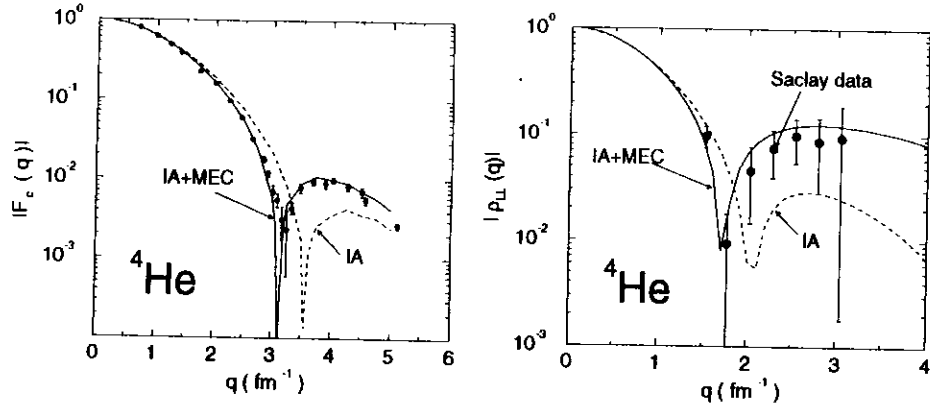


FIG. 2. The  ${}^4\text{He}$  charge form factor (left panel) and longitudinal-longitudinal distribution function (right panel).

three-body charge and current operators, such as those arising from  $\Delta$ -excitation. Such studies are in progress.

## MONTE CARLO METHODS AND FEW-NUCLEON SYSTEMS

Stochastic calculations of bound and continuum states of light nuclei with realistic interactions and currents have been carried out within two approaches: Variational Monte Carlo (VMC) and Green's Function Monte Carlo (GFMC).

In the VMC method, the nuclear wave function is expressed as

$$\psi(\mathbf{R}) = \sum_{n=1, N} \psi_n(\mathbf{R}) |n\rangle, \quad \mathbf{R} \equiv \mathbf{r}_1, \dots, \mathbf{r}_A, \quad (12)$$

where  $|n\rangle$  denote the spin-isospin states of the  $A$  nucleons, their total number  $N$  being given by  $N = 2^A A! / [(A-Z)! Z!]$ . Here  $2^A$  comes from the spin degeneracy, while the smaller binomial coefficient suffices for the isospin degeneracy, due to charge conservation. In this representation, an operator  $O$  is a matrix function  $[O_{mn}(\mathbf{R})]$  of dimension  $N \times N$ . The expectation value is written as

$$\frac{\langle \psi | O | \psi \rangle}{\langle \psi | \psi \rangle} = \int d\mathbf{R} P(\mathbf{R}) \frac{\psi_m^*(\mathbf{R}) O_{mn}(\mathbf{R}) \psi_n(\mathbf{R})}{P(\mathbf{R})}, \quad (13)$$

where  $P(\mathbf{R})$ ,

$$P(\mathbf{R}) = \frac{\sum_n |\psi_n(\mathbf{R})|^2}{\int d\mathbf{R} \psi^\dagger(\mathbf{R}) \psi(\mathbf{R})}, \quad (14)$$

can be interpreted as a probability density. If  $\mathbf{R}_1, \dots, \mathbf{R}_L$  are  $L$  configurations drawn from  $P(\mathbf{R})$ , e.g., according to the Metropolis algorithm [26], then

$$\langle O \rangle \simeq \frac{1}{L} \sum_i \frac{\psi_m^* O_{mn} \psi_n}{P} \Big|_{\mathbf{R}_i}. \quad (15)$$

The statistical error associated with the sampling is  $\sigma/\sqrt{L}$ , where  $\sigma$  is a calculable constant.

The main advantage of this technique is that matrix elements of operators can be calculated in an exact fashion even when they contain many-body terms with intricate spin-isospin dependence, as those occurring, for example, in the two-body current operators or Hamiltonian. The method is very general, and can be used with any wave function, such as Faddeev (F) or Correlated Hyperspherical Harmonics (CHH), or also to calculate transition matrix elements (with a suitable choice of  $P(\mathbf{R})$ ). However, the size of the arrays grows very rapidly with  $A$ , and present day computers restrict the application of the VMC method in the form discussed here to nuclei with  $A \leq 8$ . In the last few years VMC methods and cluster expansion techniques have been successfully used to calculate ground state properties of larger nuclei, such as  ${}^{16}\text{O}$  [27] and  ${}^{40}\text{Ca}$  [28] with reasonable accuracy.

In the GFMC method stochastic techniques are used to sample the imaginary time propagator  $\exp(-\tau H)$  [29,30]. This permits the evaluation of matrix elements, such as

$$\langle H(\tau) \rangle = \frac{\langle \psi_T | H e^{-\tau H} | \psi_T \rangle}{\langle \psi_T | e^{-\tau H} | \psi_T \rangle}, \quad (16)$$

for which, in the limit of large  $\tau$ ,  $\langle H(\tau) \rangle \rightarrow E_0$ , the ground-state energy of the system. Here  $\psi_T$  is a trial state having a non-vanishing overlap with the ground state. Of course, the method is easily generalized to calculate the energies of low-lying states by judicious choice of the trial state. The rate of convergence with  $\tau$  depends on both the nature of the energy spectrum (the energy spacing) as well as on the quality of the trial wave function. By dividing the time  $\tau$  into  $K$  small steps  $\delta\tau$ ,  $\exp(-\tau H)$  can be written in configuration space as:

$$\langle \mathbf{R}' | e^{-\tau H} | \mathbf{R} \rangle = \int \left[ \prod_{k=1}^K d\mathbf{R}_k \right] G(\mathbf{R}', \mathbf{R}_K) \left[ \prod_{k=2}^K G(\mathbf{R}_k, \mathbf{R}_{k-1}) \right] G(\mathbf{R}_1, \mathbf{R}), \quad (17)$$

where

$$G(\mathbf{R}_k, \mathbf{R}_{k-1}) = \langle \mathbf{R}_k | e^{-\delta\tau H} | \mathbf{R}_{k-1} \rangle . \quad (18)$$

Stochastic methods are used to solve iteratively the integral equation

$$\psi^{(k+1)}(\mathbf{R}') = \int d\mathbf{R} G(\mathbf{R}', \mathbf{R}) \psi^{(k)}(\mathbf{R}) . \quad (19)$$

The kernel is interpreted as a conditional probability for a configuration to evolve from  $\mathbf{R}$  at  $\tau$  to  $\mathbf{R}'$  at  $\tau + \delta\tau$ . This conditional probability in the limit of small  $\delta\tau$  can be approximated into a product of kinetic and potential energy terms

$$\begin{aligned} G(\mathbf{R}', \mathbf{R}) &\simeq e^{-(\delta\tau/2)V(\mathbf{R}')} \langle \mathbf{R}' | e^{-\delta\tau T} | \mathbf{R} \rangle e^{-(\delta\tau/2)V(\mathbf{R})} \\ &\equiv W(\mathbf{R}', \mathbf{R}) \left( \frac{1}{2\pi} \frac{m}{\delta\tau} \right)^{3A/2} \exp\left[ -\frac{m}{2\delta\tau} (\mathbf{R}' - \mathbf{R})^2 \right] . \end{aligned} \quad (20)$$

The kinetic energy term acts to diffuse the system around  $\mathbf{R}$  through a normalized Gaussian distribution with variance  $\delta\tau/m$ , while the potential energy term acts to keep the system in regions of space where the potential energy is most negative by enhancing the probability for jumps to occur at such locations. The algorithm for evolving a configuration from  $\mathbf{R}$  to  $\mathbf{R}'$  consists in sampling a new configuration  $\mathbf{R}'$  with probability proportional to  $\exp[-(m/2\delta\tau)(\mathbf{R}' - \mathbf{R})^2]$ , and weighing the importance of this configuration with  $W(\mathbf{R}', \mathbf{R})$ . One way to effect this weighing is to replicate or delete configurations with probability proportional to  $W(\mathbf{R}', \mathbf{R})$ . In this way a new ensemble of configurations at  $\tau + \delta\tau$  is generated. The initial ensemble of configurations is distributed according to  $\psi_T(\mathbf{R})$ . The algorithm just described is the simplest implementation of GFMC. More sophisticated approximations for the short-time propagators as well as importance sampling techniques are used in the actual simulations [29]. Spin and isospin degrees of freedom render the nuclear problem technically more involved.

## THE LOW-ENERGY CONTINUUM

Both VMC and GFMC techniques have been used to study the few-nucleon continuum at very low energies. To illustrate the method [31], suppose we have two clusters of radii  $R_1$  and  $R_2$ . When the two clusters are well separated ( $R \gg R_1 + R_2$ ) the Hamiltonian is given by

$$H = H_1 + H_2 + H_{\text{rel}} , \quad (21)$$

where  $H_i$  is the Hamiltonian describing cluster  $i$  and  $H_{\text{rel}}$  is the relative kinetic energy

$$H_{\text{rel}} = -\frac{1}{2\mu} \nabla_R^2 , \quad (22)$$

$\mu$  being the reduced mass. In this asymptotic region  $\psi$  factorizes as  $\psi_1 \psi_2 \psi_{\text{rel}}(\mathbf{R})$ , where  $\psi_i$  is the wave function relative to cluster  $i$ , and

$$\psi_{\text{rel}}(\mathbf{R}) = [j_l(kR) - \text{tg}\delta_l(k) n_l(kR)] y_{lm}(\hat{\mathbf{R}}) , \quad (23)$$

where  $k = \sqrt{2\mu E_{\text{rel}}}$ . For simplicity, only single channel problems are dealt with in the present discussion (although, the method can be generalized to treat multi-channel problems). In order to determine the phase shift  $\delta_l$  as function of energy, we fix a radius  $R$  in the asymptotic region and a value  $b = \mathbf{R} \cdot \nabla_R \psi / \psi|_R$  for the logarithmic derivative. We then solve for the energy and bound state wave function (with the prescribed  $b$ ) of the system  $1 + 2$  confined in a region of radius  $R$ . By varying  $b$ , the curve  $E_{\text{rel}}(b) = E(b) - E_1 - E_2$  is obtained, which can be inverted to yield  $b = b(E_{\text{rel}})$ , and hence the phase shift.

The method is best suited to describe very low-energy scattering, since at higher energies the state  $\psi$  has to be orthogonalized to all other states with lower energies (and possibly to bound states, if these are present in the particular channel under consideration). This is difficult to do in VMC or GFMC calculations.

The VMC method has been used to study the low-lying resonances in  ${}^4\text{He}$  [31], the  $n + {}^4\text{He}$  P-wave resonances [32,33], the S-wave  $J^\pi = 1^+ n + {}^3\text{He}$  and  $p + {}^3\text{He}$  scattering lengths [21,34], and the S-wave  $J^\pi = 2^+ d + d$  scattering at energies below 500 keV [35]. The  ${}^5\text{He}$  resonances have also been studied with the GFMC method [33].

The calculated values for the  $n + {}^3\text{He}$  and  $p + {}^3\text{He}$  scattering lengths are  $(3.50 \pm 0.25)$  fm and  $(10.1 \pm 0.5)$  fm, in agreement with the empirical values  $(3.52 \pm 0.25)$  fm and  $(10.2 \pm 1.4)$  fm. The  $n + {}^3\text{He}$  scattering length is above the value  $(3.25 \pm 0.10)$  fm obtained from a R-matrix analysis of the experimental data [36]. In principle, the  $n + {}^3\text{He}$  channel is coupled to the  $p + t$  channel as well as to the  $n + {}^3\text{He}$  and  $p + t$  channels in relative D-waves. These couplings in the present VMC calculation have been ignored; the R-matrix analysis as well as theoretical estimates indicate that they are small [36].

The cross sections for the reactions  $n + {}^3\text{He} \rightarrow {}^4\text{He} + \gamma$  at thermal neutron energies and  $p + {}^3\text{He} \rightarrow {}^4\text{He} + e^+ + \nu_e$  at keV proton energies have been calculated with the VMC wave functions corresponding to the Argonne  $v_{14}$  and Urbana model-VII TNI (model-VII is a more attractive version of model-VIII) [21,34,37]. The two most recent measurements of the radiative capture,  $(55 \pm 3) \mu\text{b}$  [38]

and  $(54 \pm 6) \mu\text{b}$  [39], are somewhat smaller than the calculated value of  $85.9 \mu\text{b}$  [37]. The  ${}^3\text{He}(p, e^+\nu_e){}^4\text{He}$  cross section cannot be measured in the energy range relevant for solar fusion. However, the calculated value is much smaller than that predicted on the basis of shell model descriptions of the initial and final states. Indeed, the astrophysical S-factor is found to be  $1.44 \times 10^{-23} \text{ MeV-b}$  [37] rather than the value  $8 \times 10^{-23} \text{ MeV-b}$  quoted in the recent review by Bahcall and Ulrich [40], leading to a significantly smaller neutrino flux associated with this reaction.

These reactions are interesting in that their cross sections are very sensitive to the model used to describe both the ground state and continuum wave functions, and the two-body electromagnetic and weak current operators. This is because the single-nucleon magnetic dipole or Gamow-Teller operators cannot connect the dominant S-wave components of the  ${}^3\text{He}$  and  ${}^4\text{He}$  wave functions at low energy. Hence, in impulse approximation the calculated cross section is small, as the reaction must proceed through the small components of the wave functions. Indeed,  $\sigma_{IA}(n + {}^3\text{He})$  is found to be  $5.7 \mu\text{b}$ , about 7% of the total calculated value and about 10% of the empirical value. However, two-body currents can connect the S-wave components, and their matrix element is exceptionally large. Furthermore, the cross sections are sensitive to the scattering length and the tensor force [21,34]. It will be interesting to repeat these calculations with the presumably more accurate CHH bound and continuum wave functions [4,7] and the more recent  $\nu_{18}$  interaction with a weaker tensor force than the present  $\nu_{14}$ . Work along these lines is in progress.

The P-wave resonances in  ${}^5\text{He}$  have been studied with GFMC and the Argonne  $\nu_{14}$  and Urbana model-VIII Hamiltonian [33]. The energies  $\langle E(\tau; 3^-/2) \rangle$  and  $\langle E(\tau; 1^-/2) \rangle$  of the  $J^\pi = 3^-/2$  and  $1^-/2$  states are shown in Fig. 3 relative to the  $\alpha$ -particle ground state energy.

From the experimental phase shift at a certain energy a given channel radius  $R$  corresponding to the node location in the relative  $n + {}^4\text{He}$  wave function is easily determined. The ‘‘experimental’’ energies plotted in Fig. 3 correspond to  $R=12.5 \text{ fm}$ .

The predicted splitting between the  $3/2$  and  $1/2$  states is in good agreement with the observed one, although the individual energies are somewhat higher than the empirical values. The TNI gives a significant contribution to the splitting, and it will be interesting to investigate the effects of a TNI with a more realistic treatment of the repulsive part. In addition, the dependence of these results on the underlying two-nucleon interaction is being investigated.

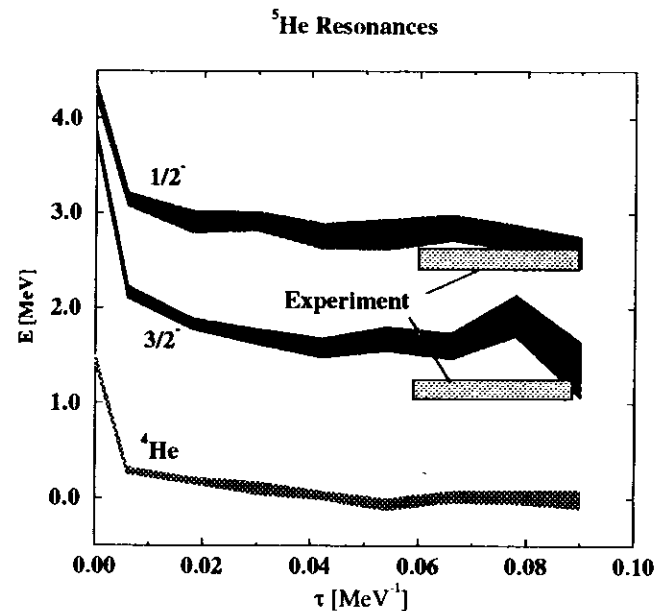


FIG. 3. The  ${}^5\text{He}$  P-wave resonances.

## THE CONTINUUM AT INTERMEDIATE ENERGIES

### Inclusive Scattering

GFMC methods are useful not only in studying the low-energy properties of many-body systems, corresponding to the large  $\tau$  limit of the propagator, but also their properties at higher excitation energies corresponding to the short and intermediate  $\tau$  limits of the propagator.

Inclusive inelastic scattering by a weakly coupled external probe transferring momentum  $\mathbf{q}$  and energy  $\omega$  to the nucleus is characterized by a response function

$$S(q, \omega) = \sum_{n \neq 0} |\langle n | O(\mathbf{q}) | 0 \rangle|^2 \delta(\omega + E_0 - E_n), \quad (24)$$

where  $|n\rangle$  and  $E_n$  are the eigenstates and eigenenergies of the Hamiltonian, and  $O(\mathbf{q})$  denotes the nature of the coupling. For example, in  $(e, e')$  scattering  $O(\mathbf{q})$  is either the nuclear charge or current operator, while in  $(\vec{p}, \vec{n})$  reactions one attempts to extract the response to the couplings

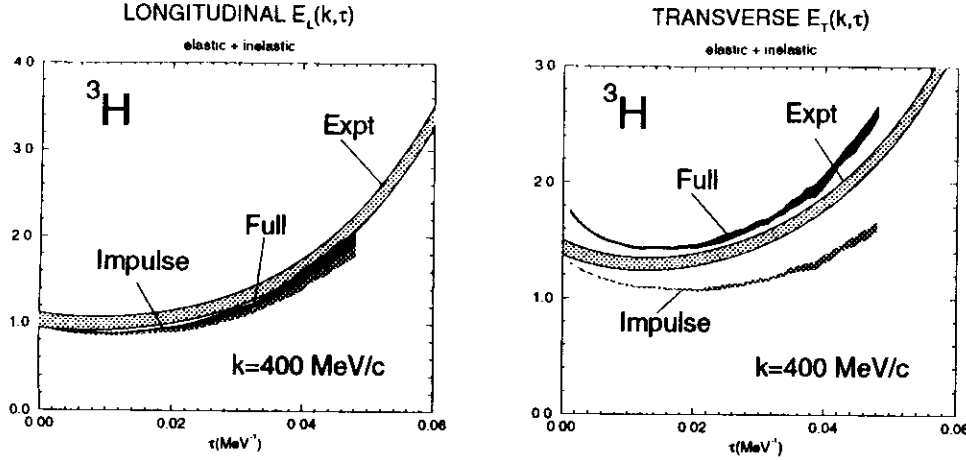


FIG. 4.  ${}^3\text{H}$  Euclidean responses at 400 MeV/c .

$$\rho_{\sigma\tau,L}(\mathbf{q}) = \sum_i \sigma_i \cdot \hat{\mathbf{q}} \tau_{\pm,i} e^{i\mathbf{q} \cdot \mathbf{r}_i}, \quad (25)$$

and

$$\rho_{\sigma\tau,T}(\mathbf{q}) = \sum_i \sigma_i \times \hat{\mathbf{q}} \tau_{\pm,i} e^{i\mathbf{q} \cdot \mathbf{r}_i}. \quad (26)$$

One should bear in mind, however, that hadronic probes do not couple weakly to the nucleus, and therefore care should be taken in comparing the experimental data with the results of calculations based on the above couplings.

Response functions are difficult to calculate, as they require a knowledge of both the bound and continuum spectra of the nucleus. Indeed, the deuteron is the only system for which accurate calculations of the electromagnetic and charge exchange responses [41,42] have been carried out based on realistic interaction models. Calculations of the  $A > 2$  responses have been performed in plane-wave-impulse-approximation (PWIA), i.e., by approximating the final states with plane waves and by neglecting the contributions of two-body components in the electro-excitation operator [43,44]. Within this approach, the longitudinal and transverse responses measured in  $(e,e')$  scattering are given by

$$S_{L,T}^{\text{PWIA}}(q, \omega) = C_{L,T} \int d\mathbf{p} \int_{E_{\text{th}}}^{\infty} dE \delta \left[ \omega - E - \frac{(\mathbf{p} + \mathbf{q})^2}{2m} - \frac{p^2}{2m_{A-1}} \right] P(\mathbf{p}, E), \quad (27)$$

where  $P(\mathbf{p}, E)$  is the spectral function

$$P(\mathbf{p}, E) = \sum_{n(A-1)} |\langle n(A-1) | a(\mathbf{p}) | 0 \rangle|^2 \delta[E + E_0 - E_{n(A-1)}]. \quad (28)$$

Here, the constants  $C_{L,T}$  represent essentially the strengths of the single-nucleon couplings, the  $|n(A-1)\rangle$  and  $E_{n(A-1)}$  are the eigenstates and eigenenergies of the  $(A-1)$  Hamiltonian, and  $a(\mathbf{p})$  is the annihilation operator for a nucleon with momentum  $\mathbf{p}$ . It is easily seen that in PWIA: i) the Coulomb sum

$$\frac{1}{C_L} \int_0^{\infty} d\omega S_L^{\text{PWIA}}(q, \omega) = 1, \quad (29)$$

independent of momentum transfer, and ii) the ratio

$$\left. \frac{C_T S_L(q, \omega)}{C_L S_T(q, \omega)} \right|_{\text{PWIA}} = 1. \quad (30)$$

Both these predictions are inconsistent with data at intermediate values of momentum transfer. For example, the empirical ratio is much less than one in the quasielastic peak region, particularly so in heavier nuclei.

In the GFMC approach [41], one considers Euclidean response functions defined as the Laplace transform of  $S(q, \omega)$

$$\begin{aligned} E(q, \tau) &= \int_0^{\infty} d\omega e^{-\tau\omega} S(q, \omega) \\ &= \langle 0 | O^\dagger(\mathbf{q}) e^{-\tau(H-E_0)} O(\mathbf{q}) | 0 \rangle - e^{-\tau\omega_{\text{el}}} \langle 0 | O(\mathbf{q}) | 0 \rangle^2, \end{aligned} \quad (31)$$

where  $\omega_{\text{el}}$  is the energy of the recoiling ground state. At  $\tau=0$  the Euclidean response is simply the sum rule, while derivatives with respect to  $\tau$  correspond to energy-weighted sum rules. For finite  $\tau$ , the  $E(q, \tau)$  provides a measure of the energy distribution. As  $\tau$  increases, the higher energy components of the system are gradually suppressed, until one is eventually left with the threshold response.

The calculated Euclidean responses of  ${}^3\text{H}$  and  ${}^3\text{He}$  at  $q=400$  MeV/c, and of  ${}^4\text{He}$  at  $q=300$  MeV/c [45,46] are compared with the experimental  $E^{\text{exp}}(q, \tau)$  in Figs. 4-6. The Argonne  $\nu_8$ +Urbana model-VIII TNI have been employed in these simulations. We note that the  ${}^3\text{H}$  and  ${}^3\text{He}$  responses include both the elastic and inelastic contributions [46]. We show the Saclay [47] (Bates [48]) data for  ${}^3\text{He}$  ( ${}^3\text{H}$ ) and both the Saclay [49] and Bates [50] data for  ${}^4\text{He}$ . The Bates data [48] for  ${}^3\text{He}$  are consistent with the Saclay ones [47], and are not displayed.

The  $E^{\text{exp}}(q, \tau)$  is obtained by simply Laplace-transforming the data. These are available only up to a maximum energy  $\omega_{\text{max}}$ . In the longitudinal channel we have estimated the unobserved strength at  $\omega > \omega_{\text{max}}$  by means of sum rule

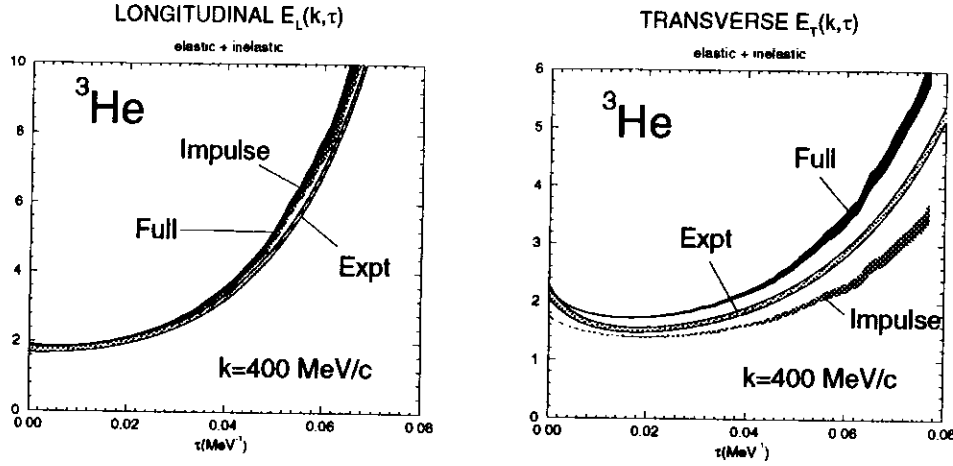


FIG. 5.  ${}^3\text{He}$  Euclidean responses at 400 MeV/c .

techniques [24]. The effect of including this high-energy strength in  $E_L^{\text{exp}}(q, \tau)$  is shown for the  $\alpha$ -particle in Fig. 6 by the curve labelled “extrapolated”. It decreases rapidly with  $\tau$  because of the exponential damping factor  $\exp(-\tau\omega)$ , and is negligible for  $\tau \gtrsim 0.015 \text{ MeV}^{-1}$ . In the transverse channel, we simply show the experimental results corresponding to the truncated  $S_T(q, \omega)$ . Since the Saclay measurements extend to higher  $\omega$ , they naturally lead to an increased  $E_T^{\text{exp}}(q, \omega)$  near  $\tau=0$ . Again though, the effects of this high energy strength (mostly due to the  $\Delta$ -resonance) are rapidly suppressed at finite  $\tau$ , so that the Bates and Saclay measurements are nearly identical by  $\tau \simeq 0.02 \text{ MeV}^{-1}$ .

We note that in obtaining the elastic+inelastic trinucleon  $E_{L,T}^{\text{exp}}$  we have used the appropriate experimental form factors. The elastic contribution for  $\tau \gtrsim 0.06 \text{ MeV}^{-1}$  is large.

The longitudinal data for the helium isotopes are well reproduced by the calculations. There is, however, a 10% discrepancy between theory and experiment in the  ${}^3\text{H}$  longitudinal channel. Since the charge form factor of tritium is in agreement with the present theory [19], this discrepancy can be traced back to excess strength present in the inelastic data. This is consistent with the analysis of the  ${}^3\text{H}$  Coulomb sum rule carried out in [24]. At the low momentum transfers considered, two-body charge operators give small corrections. The  $E_L^{\text{PWIA}}$  (shown only for the  $\alpha$ -particle) has the incorrect  $\tau$ -dependence, and far more strength than observed.

In the transverse channel two-body currents have a rather large effect. In the

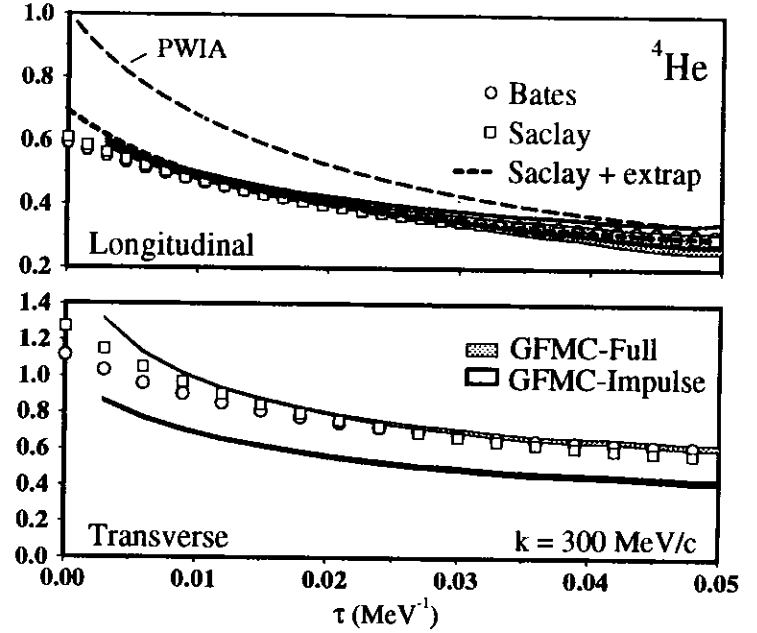


FIG. 6.  ${}^4\text{He}$  Euclidean responses at 300 MeV/c .

$\alpha$ -particle they account for more than 30% of the measured response even at large  $\tau$ , where the latter is mostly sensitive to strength in the quasielastic and threshold regions of  $S_T(q, \omega)$ . In the  $A=3$  systems two-body current contributions are also significant. However, their inclusion appears to lead to a 5-10 % overprediction of the data for  $\tau \gtrsim 0.02 \text{ MeV}^{-1}$ . Since the magnetic form factors are in agreement with theory [19], this discrepancy must be due to excess strength produced by theory in the inelastic channel. At this point the origin of this discrepancy is not clear.

A final comment is now in order. The theoretical framework employed here does not include pion production nor a dynamic treatment of the  $\Delta$ -resonance, and hence cannot explain the response in the  $\Delta$ -peak region, corresponding to  $\tau \lesssim 0.02 \text{ MeV}^{-1}$ . However, for large values of  $\tau$  a static parametrization of the currents associated with virtual  $\Delta$ -production, such as the one used in the present work should be adequate, since the product  $\tau\delta E \gg 1$ , where  $\delta E$  is a typical  $N \rightarrow \Delta$  excitation energy.

We conclude this subsection by reporting the results obtained with the sim-

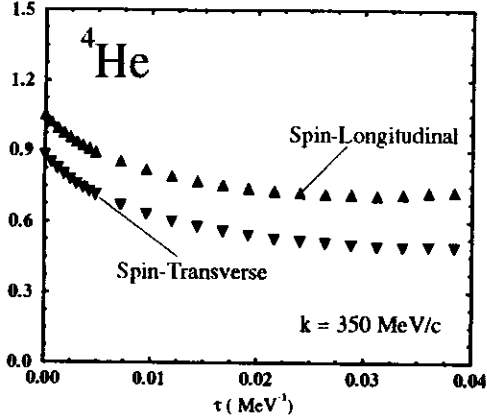


FIG. 7.  ${}^4\text{He}$  Euclidean spin-longitudinal and spin-transverse responses at 350 MeV/c.

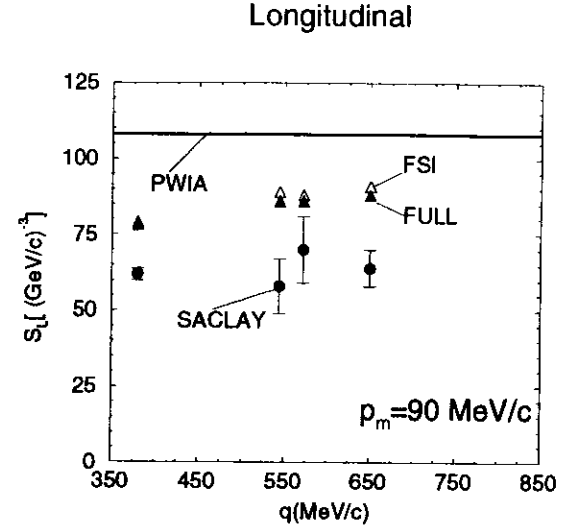
ple couplings  $\rho_{\sigma\tau,L}$  and  $\rho_{\sigma\tau,T}$  given above for the spin-longitudinal and spin-transverse response functions of the  $\alpha$ -particle [42], Fig. 7. These can be extracted from measurements of quasielastic  $(\vec{p}, \vec{n})$  reactions. At present no data are available for  ${}^4\text{He}$ . However, experiments carried out on  ${}^{12}\text{C}$  and  ${}^{40}\text{Ca}$  show that, contrary to theoretical expectations [42], no indication is found for the enhancement of  $E_{\sigma\tau,L}$  with respect to  $E_{\sigma\tau,T}$  [51].

### Exclusive Scattering

It is not possible to use GFMC methods in the present form to describe exclusive reactions, such as  ${}^3\text{He}(e, e'p)d$  or  ${}^4\text{He}(e, e'p)t$ . Faddeev techniques are employed to study three-body reactions [8]. However, it is not clear whether Faddeev-Yakubovsky schemes can be extended to treat reactions involving four nucleons at moderate and high excitation energies.

In the Orthogonal Correlated States (OCS) approach [52–54] we write the  $(A-1)+1$  wave function as

$$\psi^{\text{CS}}(\mathbf{p}) = \mathcal{A}[\mathcal{S} \prod_{i=1}^A F_{i,A}] \psi_{A-1}(\mathbf{r}_1, \dots, \mathbf{r}_{A-1}) \phi_{\mathbf{p}}(\mathbf{r}_A), \quad (32)$$



where  $\mathcal{S}$  and  $\mathcal{A}$  are, respectively, the symmetrizer and antisymmetrizer,  $\psi_{A-1}$  is the  $(A-1)$  bound state wave function,  $\phi_{\mathbf{p}}$  is the nucleon wave function with momentum  $\mathbf{p}$  relative to the  $(A-1)$  cluster, and  $F_{i,A}$  is the correlation operator between nucleon  $i$  in the residual system and nucleon  $A$ . The correlation operator is momentum- (or energy-) independent, and is such that  $F_{i,A} \rightarrow 1$ , when  $r_{i,A}$  is large [52]. The single-nucleon wave function is taken as the solution of a Schrödinger equation with a complex energy-dependent optical potential. The CS states are then orthogonalized to the ground state of the  $A$ -nucleon system, and among themselves [52],  $\psi^{\text{CS}} \rightarrow \psi^{\text{OCS}}$ .

The OCS wave functions have been used to study the  $A=3$  inclusive response [52,53], and the  ${}^4\text{He}(e, e'p)t$  reaction [54]. In Fig. 8 we compare the longitudinal and transverse reduced  ${}^4\text{He}(e, e'p)t$  cross sections in parallel kinematics with the Saclay data obtained at a fixed missing momentum  $\mathbf{p}_m (= \mathbf{p} - \mathbf{q})$  of 90 MeV/c [55]. By setting  $F_{i,A} = 1$  and  $\phi_{\mathbf{p}} = \exp[i\mathbf{p} \cdot (\mathbf{r}_A - \mathbf{R}_{A-1})]$ , and by neglecting the effects of antisymmetrization, orthogonalization and two-body charge and current operators, we obtain the PWIA curve, which is independent of momentum transfer. The curve labelled “fsi” is computed by using the OCS wave functions, but neglecting the two-body operators, while the curve labelled “full” corresponds to the full calculation.

Theory is in reasonable agreement with the transverse data. However, a 20-30% discrepancy remains between theory and experiment in the longitudinal channel. It should be emphasized that the results are sensitive to the optical

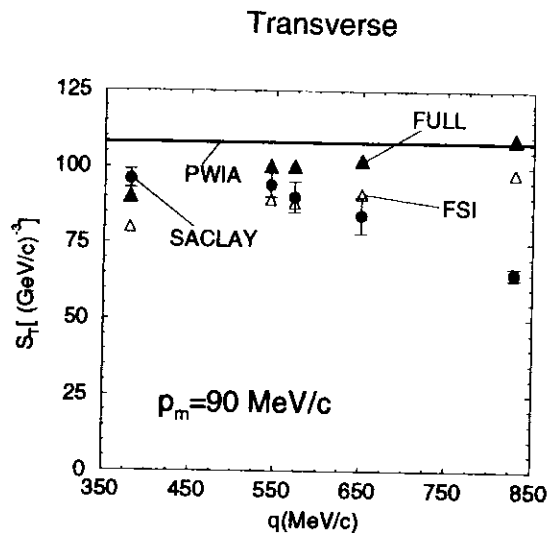


FIG. 8.  ${}^4\text{He}(e, e'p)t$  longitudinal (top panel) and transverse (bottom panel) reduced cross sections at  $p_m=90$  MeV/c.

potential, particularly to its imaginary part, used to obtain the distorted wave function, although it appears difficult to simultaneously reproduce the longitudinal and transverse data. Clearly, the use of an optical model is unsatisfactory, since the connection with the underlying nucleon-nucleon dynamics is lost.

## CONCLUSIONS

Monte Carlo methods are ideally suited for studying both structure and dynamics in light nuclei. We are proceeding with a comprehensive program to calculate properties of nuclear systems from the underlying two-body dynamics as constrained by NN scattering data. Three-nucleon interactions as well as two-body electroweak currents constructed consistently with the interaction model play an important role in these studies. The ground-state structure of S-shell nuclei seems to be reasonably well understood. However, low-energy electroweak reactions, (p,n) reactions in the quasielastic regime, as well as inclusive and exclusive electron scattering reactions at intermediate energies provide both challenges and opportunities to refine models of interactions and reaction mechanisms.

## ACKNOWLEDGMENTS

We wish to thank our colleagues A. Arriaga, V.R. Pandharipande, S.C. Pieper and D.O. Riska for many useful comments and stimulating discussions. The work of RS and JC was supported by the U.S. Department of Energy, that of RBW by the U.S. Department of Energy, Nuclear Physics Division, under contract No. W-31-109-ENG-38.

- [1] C.R. Chen, G.L. Payne, J.L. Friar and B.F. Gibson, *Phys. Rev. C* **33**, 1740 (1986).
- [2] W. Glöckle and H. Kamada, *Nucl. Phys.* **A560**, 541 (1993).
- [3] S. Ishikawa, T. Sasakawa, T. Sawada and T. Ueda, *Phys. Rev. Lett.* **53**, 1877 (1984).
- [4] A. Kievsky, M. Viviani and S. Rosati, *Nucl. Phys.* **A551**, 241 (1993).
- [5] M. Viviani, A. Kievsky and S. Rosati, CEBAF preprint TH-94-18, (1994).
- [6] D. Hüber, H. Witala and W. Glöckle, *Few-Body Systems* **14**, 171 (1993).
- [7] A. Kievsky, M. Viviani and S. Rosati, *Nucl. Phys. A* in press, (1994).
- [8] W. Glöckle, these proceedings.
- [9] D.M. Ceperley and E.L. Pollock, *Phys. Rev. Lett.* **56**, 351 (1986).
- [10] C.W. Johnson, S.E. Koonin, G.H. Lang and W.E. Ormand, *Phys. Rev. Lett.* **69**, 3157 (1992).
- [11] J. Negele, these proceedings.
- [12] M. Lacombe *et al.*, *Phys. Rev. C* **21**, 861 (1980).
- [13] R. Machleidt, *Adv. Nucl. Phys.* **19**, 189 (1989).
- [14] I.E. Lagaris and V.R. Pandharipande, *Nucl. Phys.* **A359**, 331 (1981).
- [15] R.B. Wiringa, R.A. Smith, and T.L. Ainsworth, *Phys. Rev. C* **29**, 1207 (1984).
- [16] R. Wiringa, unpublished.
- [17] J. Carlson, *Nucl. Phys.* **A522**, 185c (1991).
- [18] R. Wiringa, V. Fiks and A. Fabrocini, *Phys. Rev. C* **38**, 1010 (1988).
- [19] R.B. Wiringa, *Phys. Rev. C* **43**, 1585 (1991).
- [20] R. Schiavilla, V.R. Pandharipande, and D.O. Riska, *Phys. Rev. C* **40**, 2294 (1989).
- [21] J. Carlson, D.O. Riska, R. Schiavilla, and R.B. Wiringa, *Phys. Rev. C* **42**, 830 (1990).
- [22] R. Schiavilla, V.R. Pandharipande, and D.O. Riska, *Phys. Rev. C* **41**, 309 (1990).
- [23] R. Schiavilla and D.O. Riska, *Phys. Rev. C* **43**, 437 (1991).
- [24] R. Schiavilla, R.B. Wiringa and J. Carlson, *Phys. Rev. Lett.* **70**, 3856 (1993).
- [25] R.B. Wiringa, V.G.J. Stoks and R. Schiavilla, to be published.
- [26] N. Metropolis *et al.*, *J. Chem. Phys.* **21**, 1087 (1953).

- [27] S.C. Pieper, R.B. Wiringa, and V.R. Pandharipande, *Phys. Rev. C* **46**, 1741 (1992).
- [28] S.C. Pieper, private communication.
- [29] J. Carlson, *Phys. Rev.* **C38**, 1879 (1988).
- [30] J. Carlson, *Nucl. Phys.* **A508**, 141c (1990).
- [31] J. Carlson, V.R. Pandharipande and R.B. Wiringa, *Nucl. Phys.* **A424**, 47 (1984).
- [32] J. Carlson, K.E. Schmidt and M.H. Kalos, *Phys. Rev. C* **36**, 27 (1987).
- [33] J. Carlson and R.B. Wiringa, to be published.
- [34] J. Carlson, D.O. Riska, R. Schiavilla and R.B. Wiringa, *Phys. Rev. C* **44**, 619 (1991).
- [35] A. Arriaga, V.R. Pandharipande and R. Schiavilla, *Phys. Rev. C* **43**, 983 (1991).
- [36] G. Hale, private communication.
- [37] R. Schiavilla, R.B. Wiringa, V.R. Pandharipande and J. Carlson, *Phys. Rev. C* **45**, 2628 (1992).
- [38] R. Wervelman *et al.*, *Nucl. Phys.* **A526**, 265 (1991).
- [39] F.L.H. Wolfs *et al.*, *Phys. Rev. Lett.* **63**, 2721 (1989).
- [40] J.N. Bahcall and R.K. Ulrich, *Rev. Mod. Phys.* **60**, 297 (1988).
- [41] J. Carlson and R. Schiavilla, *Phys. Rev. Lett* **68**, 3682 (1992).
- [42] V.R. Pandharipande *et al.*, *Phys. Rev. C* **49**, 789 (1994).
- [43] H. Meier-Hajduk *et al.*, *Nucl. Phys.* **A395**, 332 (1983).
- [44] C. Ciofi degli Atti, E. Pace and G. Salmé, *Phys. Lett.* **B141**, 14 (1984).
- [45] J. Carlson and R. Schiavilla, *Phys. Rev. C* **49**, R2880 (1994).
- [46] J. Carlson and R. Schiavilla, to be published.
- [47] C. Marchand *et al.*, *Phys. Lett.* **153B**, 29 (1985).
- [48] K. Dow *et al.*, *Phys. Rev. Lett.* **61**, 1706 (1988).
- [49] J.F. Danel *et al.*, unpublished; A. Zghiche *et al.*, Saclay preprint (1993).
- [50] K.F. von Reden *et al.*, *Phys. Rev.* **C41**, 1084 (1990).
- [51] J.B. McClelland *et al.*, *Phys. Rev. Lett.* **69**, 582 (1992).
- [52] R. Schiavilla and V.R. Pandharipande, *Phys. Rev. C* **36**, 2221 (1987).
- [53] R. Schiavilla, *Phys. Lett.* **218B**, 1 (1989).
- [54] R. Schiavilla, *Phys. Rev. Lett.* **65**, 835 (1990).
- [55] A. Magnon *et al.*, *Phys. Lett.* **222B**, 352 (1989).